Optica Applicata, Vol. LIII, No. 2, 2023
DOI: 10.37190/oa230202

Research on composite manufacturing method of semi-buried 1×32 optical splitter

Qing Tao[1,2], Sihao Xie[1,2,*]

[1]School of Mechanical Engineering, Hubei University of Technology, Wuhan 430068, China

[2]Hubei Key Laboratory of Modern Manufacturing Quantity Engineering, School of Mechanical Engineering, Hubei University of Technology, Wuhan, Hubei, P.R.China, 430068

In this paper, a composite manufacturing method was proposed to reduce the inner surface roughness of silica groove. Firstly, femtosecond laser was used to ablate the silica groove, then, a 5% concentration hydrofluoric acid solution was used to corrode the inner surface of silica groove. Secondly, Su8 adhesive was filled with the groove to form a semi-buried 1×32 optical splitter by doctor blade. The test results showed that the surface roughness Ra was less than 0.2 μm, and average insertion loss of output ports was 21.34 dB, moreover, the uniformity was less than 1.44 dB. Compared with the traditional femtosecond laser ablating method, surface roughness reduced by at least 0.1 μm, and the average insertion loss of output ports was reduced by 1.22 dB, and the uniformity was reduced by 0.41 dB. So, the composite manufacturing method improved the communication performance. It is satisfied with the requirements for optical interconnection in the electro-optical printed circuit boards.

Keywords: optical splitter, composite manufacturing method, EOPCB.

1. Introduction

With the development of communication technology, optical interconnection in the electro-optical printed circuit boards (EOPCB) [1–3] had been continuously developed. Photolithography and electron beam were common methods for fabricating optical devices for optical interconnection, but they involved complex processing [4–10] and apparatuses were expensive, so, UV laser or CO_2 laser were used to replace them [11, 12]. However, these lasers were long pulse, which mainly relied on focusing to form high energy densities for high-temperature ablation of optical material and existing diffraction limits. To overcome the shortcoming, ultrashort pulses had been gradually developed. The femtosecond (fs) laser was one of the most novel methods that could be used to process various material [13]. In particular, fs laser had ultrashort pulse width ~10^{-15} s, ultrahigh peak power ~10^{14} W/cm^2. Based on these features, it had unparal-

leled advantages compared with long-pulse lasers such as structural changes in a very small area, higher quality of ablation surface and breaking the diffraction limit. These were because of almost negligible thermal effect. Based on proposed superiority, some microstructures could be applied to form various optical devices by using fs laser [14]. Among these devices, optical splitters, which could switch the optical signal from single input to multiple outputs, acted as essential elements for integrated photonic circuits. Using femtosecond laser ablating with different parameters, the surface roughness of optical components after ablation would be different, and this difference would also affect the optical communication performance. In order to reduce surface roughness and improve the performance of optical components, a new composite manufacturing method was used. Firstly, a femtosecond laser was used to ablate the silica substrate, then, a low-concentration hydrofluoric acid solution was used to corrode the inner surface of silica groove. Then, Su8 adhesive was filled with the groove to form a semi-buried 1×32 optical splitter. This method had higher precision and good consistency [15–17]. Testing results met the high integration requirements of the EOPCB.

2. Design and analysis of optical splitter

2.1. Structure of semi-buried optical splitter

The beam propagation method (BPM) [18] was the most widely used propagation technique for modeling integrated and waveguide devices. Since the light wave was a kind of electromagnetic wave, its electric field could be written as

$$E(x, y, z, t) = \varphi(x, y, z)\exp(-i\omega t) \tag{1}$$

The scalar field allowed the wave equation to be written in the form of the well-known Helmholtz equation for monochromatic waves:

$$\frac{\partial^2 \varphi}{\partial x^2} + \frac{\partial^2 \varphi}{\partial y^2} + \frac{\partial^2 \varphi}{\partial z^2} + k_0^2 n^2(x, y, z)\varphi = 0 \tag{2}$$

where $k_0 = 2\pi/\lambda$, and $n(x, y, z)$ denotes the refractive index distribution. The most rapid variation in the field was the phase change due to propagation along the z direction, it was beneficial to factor this rapid variation out of the problem by introducing a slowly varying field $u(x, y, z)$ via the ansatz:

$$\varphi(x, y, z)\exp(-i\omega t) = u(x, y, z)\exp(i\bar{k}z) \tag{3}$$

where $\bar{k} = \bar{n}k_0$, and $\bar{n}$ was a reference refractive index. Introducing the Eq. (3) into the Helmholtz equation yielded the following equation for the slowly varying field:

$$\frac{\partial^2 u}{\partial z^2} + 2i\bar{k}\frac{\partial u}{\partial z} + \frac{\partial^2 u}{\partial x^2} + \frac{\partial^2 u}{\partial y^2}\left[k_0^2 n^2(x, y, z) - \bar{k}^2\right]u = 0 \tag{4}$$

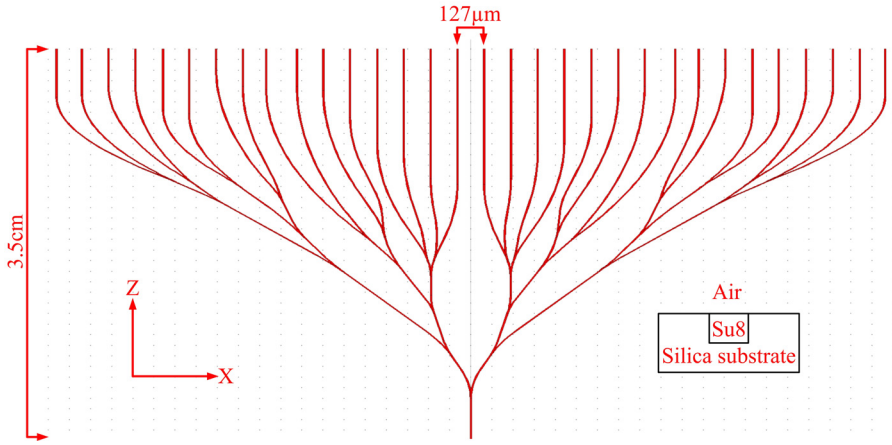

Fig. 1. Structure of semi-buried optical splitter.

Assuming that the variation of u with z was sufficiently slow so the first term could be neglected with respect to the second. The above equation became:

$$\frac{\partial u}{\partial z} = \frac{i}{2\bar{k}}\left\{\frac{\partial^2 u}{\partial x^2} + \frac{\partial^2 u}{\partial y^2} + \left[k_0^2 n^2(x, y, z) - \bar{k}^2\right]u\right\} \tag{5}$$

This was the basic BPM equation in three dimensions. Given an input field, $u(x, y, 0)$, the above equation determined the evolution of field in the space $z > 0$. The 1×32 optical splitter was designed in Fig. 1. It consisted of multiple Y-branch waveguides and straight waveguides. The Y-branch and straight waveguides could improve the output uniformity if they had proper design.

A conventional Y-branch structure consisted of an input waveguide and two branching waveguides. The two branching waveguides had the shape of S bend. SCHLAAK *et al.* [19] had simulated the bend loss of Y-branch with kinds of S-bend branching waveguides, and the results indicated that the Y-branch with raised cosine-arc branching waveguides had the lowest bend loss. The raised cosine-arc was expressed as

$$y(x) = H\left[1 - \cos\left(\frac{\pi}{L}x\right)\right] \tag{6}$$

where H was the raising height, and L was the branching length. The larger was curvature radius of raised cosine-arc, the lower was bend loss. The design parameters of semi-buried optical splitter were as followed [20,21]. The upper cladding of optical splitter was air, and its refractive index was 1 at 1550 nm. The other cladding was silica with a refractive index 1.45 at 1550 nm. The core layer was Su8 adhesive with refractive index 1.566 at 1550 nm. The length of optical splitter was 3.5 cm, the spacing of output ports was 127 μm, and the angles of all bifurcations were less than 2°. The cross -section of optical splitter was 8 μm×8 μm.

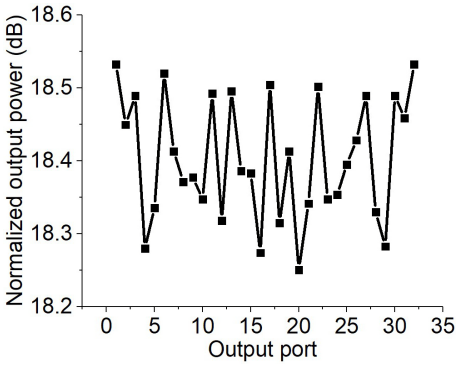

Fig. 2. The normalized output power.

The normalized output powers [22] for each output port were listed in Fig. 2. The average normalized output power was 18.403 dB, and the uniformity was 1.265 dB.

2.2. Tolerance analysis

The doctor blade method [23] was used to prepare the core layer of optical splitter, residual Su8 adhesive might remain on the surface of silica groove to form a ridged waveguide. β was the thickness of residual Su8 adhesive as shown in Fig. 3.

The uniformity [24] was an optical performance index which changed with β variation on the silica groove in Fig. 4. When the residual thickness β increased from

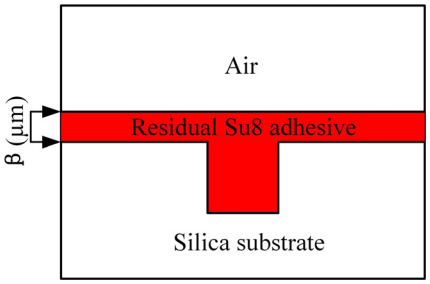

Fig. 3. The cross-section of residual Su8 adhesive.

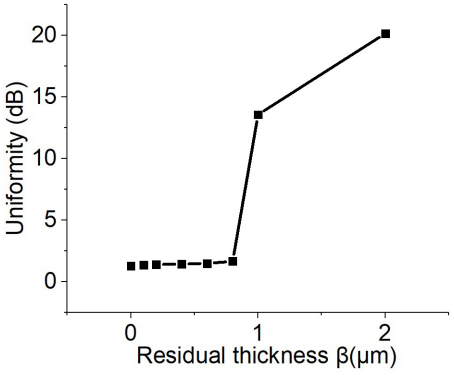

Fig. 4. The relationship between β and uniformity.

0 to 0.8 μm, the uniformity slowly increased. Specifically, when β was 0 and 0.8 μm, the uniformity was 1.3 and 1.65 dB, respectively. When the residual thickness β increased from 0.8 to 2 μm, the uniformity drastically increased. Especially β was 2 μm, the uniformity reached 20.23 dB. Therefore, the residual thickness β was preferably less than 0.8 μm in the manufacture.

3. Composite manufacturing and test method

The femtosecond laser fabricating system was illustrated in Fig. 5. The fs laser was focused on the surface of silica substrate through the half-wave plate, polarization beam splitter, reflector, and focusing objective lens, and the silica substrate was placed on a three-dimensional processing stage.

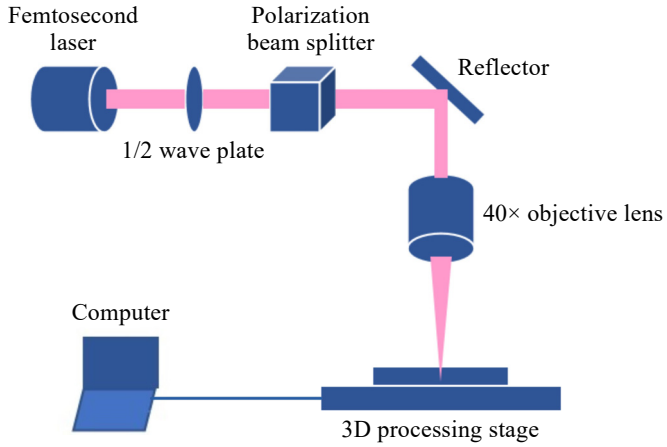

Fig. 5. The femtosecond laser fabricating system.

The translational resolution of three-dimensional processing stage was 0.1 μm, which drove the silica substrate to change position. The focusing lens was 40× with numerical aperture NA = 0.6. The femtosecond laser (Coherent Libra HE) was with a center wavelength of 800 nm, laser repetition frequency of 1 kHz, pulse width of 100 fs, beam quality factor $M^2 < 1.3$, and the focus diameter was 4 μm. The three-dimensional processing stage precisely moved according to the designed pattern and path, so that the femtosecond laser could ablate a 1×32 optical splitter groove on the silicon substrate. Then, a 5% concentration hydrofluoric acid (HF) solution was used to corrode the inner surface of groove at 100°C with a period of time. The residues and ion clusters were completely corroded in the inner surface of groove, whose surface roughness was also reduced. After that, the silica substrate would be cleaned with distilled water, and blown with nitrogen, then placed in an oven to dry. Afterwards, the Su8 adhesive was filled into the groove to form the core layer by the doctor blade method in vacuum box. The silica substrate was placed in an oven for baking, and the baking

T a b l e. Baking parameters.

Processing steps	Time	Temperature
Pre-baked	5 min	70°C
Medium bake	30 min	100°C
Post bake	60 min	120°C

parameters were listed in the Table. A semi-buried silica substrate 1×32 optical splitter was completed after baking.

The insertion loss testing method of optical splitter chip was shown in Fig. 6. The power supply switch of 650 nm light source was turned on to emit the red light. The red light passed through the fiber isolator and beam combiner to the end of single -mode fiber. The single-mode fiber was clamped on the six-dimensional coupling stage, and the optical splitter chip was fixed on the clamping stage. A white baffle was placed 0.5 cm behind the output end of optical splitter chip. The orientation and angle of single-mode fiber was adjusted, so that the coupling position of fiber and input port of optical splitter chip was the best.

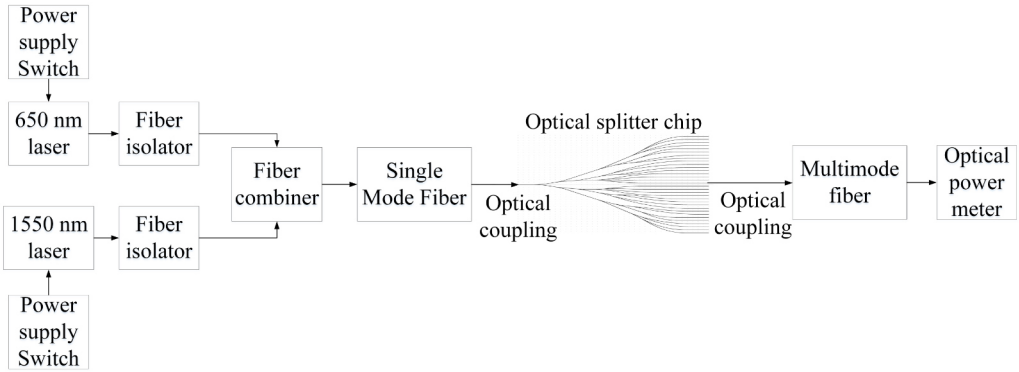

Fig. 6. Insertion loss testing method of optical splitter chip.

When 32 red light spots could be clearly seen on the white baffle and light spots were the brightest, the position and angle of single-mode fiber was fixed. Then, the power supply switch of 650 nm light source was turned off, at the same time, the power supply switch of 1550 nm light source was turned on, and the white baffle was removed. Afterwards, the orientation and angle of the six-dimensional coupling stage that clamps the multimode fiber were adjusted. The multimode fiber was aligned and coupled to the output port of optical splitter chip one-by-one, and the results of optical power meter were monitored. When the results of optical power meter were maximum value, the matching liquid was dripped on the input and output port of optical splitter chip, respectively, and the optical power values were recorded at this time. Because of matching liquid, the coupling loss at the input port and output port of optical splitter

chip were ignored, and the insertion loss value of each output ports was calculated through the following formula [25]:

$$A_i = -10\lg(P_{\text{out\_}i}/P_{\text{in}}) \tag{7}$$

where A_i referred to the insertion loss of i-th output port, $P_{\text{out\_}i}$ is the optical power of i-th output port, and P_{in} is the optical power value of input port.

4. Results and discussion

The femtosecond laser ablated the surface of silica substrate with laser power range of 10–60 mW and translational speed range of 5–20 mm/s, and ablation parameters were cross-selected. The relationship between ablation width and depth with the laser power and translational speed were obtained in Fig. 7. It was found that with the increase of laser power, the ablation width also increased in Fig. 7(a). Similarly, as the laser power increased, the ablation depth also increased in Fig. 7(b). In order to ensure that the cross-section of groove met 8 μm×8 μm, the ablation parameters were chosen: translational speed was 5 mm/s, and laser power was 40 mW.

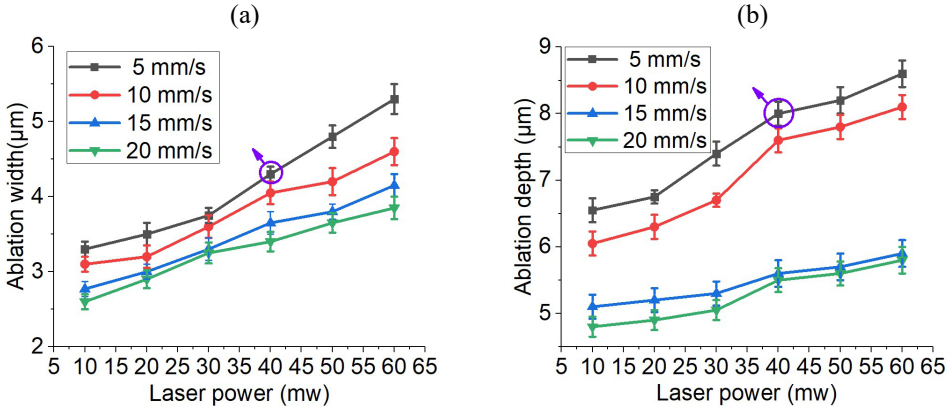

Fig. 7. The relationship between laser power and ablation (a) width and (b) depth.

In laser processing, lateral overlap ratio [26] between two adjacent ablating lines was one of the factors affecting the processing quality. The overlap ratio could be varied by changing the center distance d [27] between two adjacent ablating lines. When the center distance was different, the surface of processed area presented different textures, and the roughness of processed area characterized the removal effect.

Under the conditions of laser power (40 mW) and translational speed (5 mm/s), the variation of center distance d between two adjacent ablating lines would change the surface roughness of silica groove in Fig. 8. When d was 2.5 μm, surface roughness of groove was 1.1 μm. When d was 0.5 μm, surface roughness of groove was 0.2 μm.

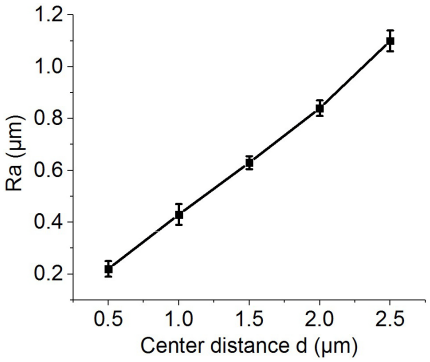

Fig. 8. The relationship between center distance *d* and roughness Ra.

When *d* varied between 0.5 and 2.5 μm, the change of surface roughness presented an approximately linear relationship. Here, the *d* was chosen as 0.5 μm. When laser power was 40 mW, and translational speed was 5 mm/s, *d* was 0.5 μm, the average width error and depth error were less than 0.1 μm in Fig. 9.

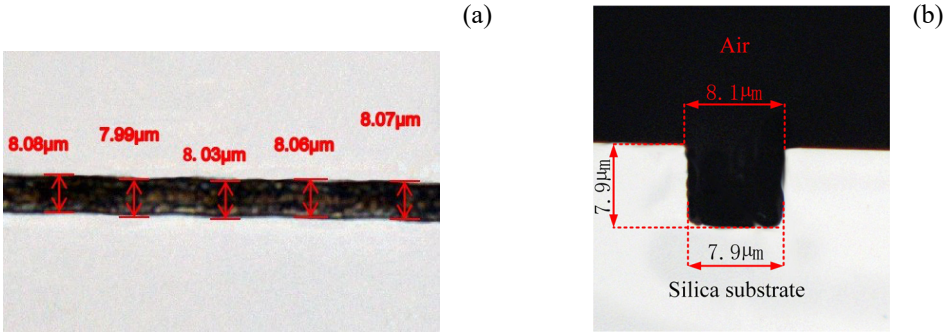

Fig. 9. 3D morphology of groove. (a) Width of groove, and (b) depth of groove.

As the corrosion time increased, the corroded thickness gradually increased in Fig. 10. The corrosion time was proportional to corroded thickness in the first 10 minutes. Although corroded thickness also increased with corrosion time, corrosion efficiency

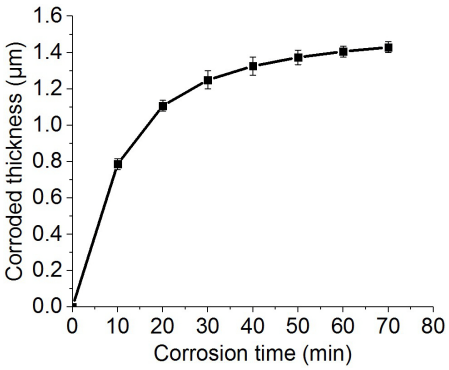

Fig. 10. The relationship between corrosion time and corroded thickness.

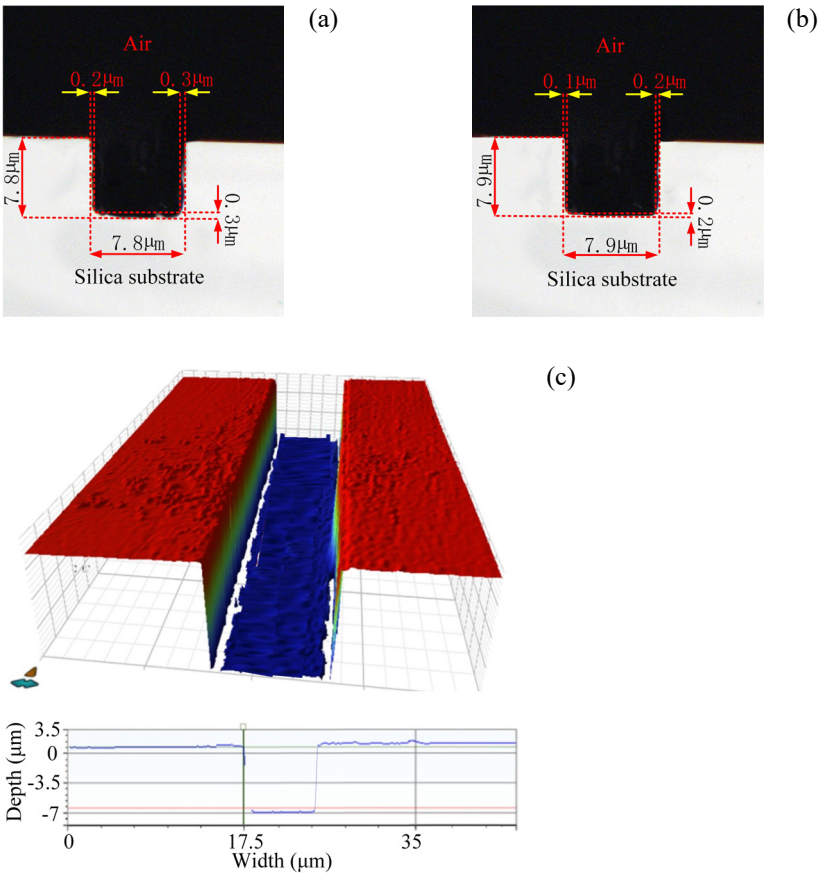

Fig. 11. The comparison of groove morphology. (a) Before corrosion, (b) after corrosion, and (c) surface morphology after corrosion.

gradually decreased and tended to stabilize during the 10–70 minutes. The corroded thickness was less than 0.2 μm during 30–70 minutes.

Therefore, two minutes were chosen to corrode the inner surface of groove to make it smooth. The comparison of morphology before corrosion and after corrosion was shown in Fig. 11. The width of groove was 7.8 μm and the depth was 7.8 μm before corrosion in Fig. 11(a). The rough thickness of left edge was 0.2 μm, the rough thickness of right edge was 0.3 μm, the rough thickness of bottom edge was 0.3 μm. After corrosion, the width of groove was 7.9 μm and the depth of groove was 7.9 μm in Fig. 11(b). The surface profile of silicon dioxide groove after corrosion was shown in Fig. 11(c). It could be clearly seen that groove was relatively smooth, and width and depth of groove were approximately 8 μm. Totally, the inner surface of groove was corroded to remove the thickness of 0.1 μm.

Thus, the experimental results shown that uniformity had an approximately linear relationship with residual thickness β in Fig. 12. When residual thickness β was

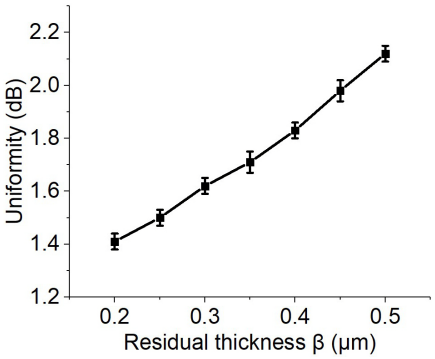

Fig. 12. The relationship between residual thickness and uniformity.

0.2 μm, the uniformity was about 1.43 dB. While residual thickness β was 0.5 μm, the uniformity was probably 2.15 dB. Therefore, the residual thickness β was preferably less than 0.2 μm to obtain better communication performance.

Moreover, the output port spacing of optical splitter was 127.1 μm, and total length of optical splitter was 3.499 cm in Fig. 13. The average insertion loss of each output port in the optical splitter was 21.34 dB, and the uniformity was less than 1.44 dB.

Under the same condition that residual thickness was less than 0.2 μm, using traditional femtosecond laser ablating method, the average insertion loss of each output port in the optical splitter was about 22.56 dB, and its uniformity was approximately

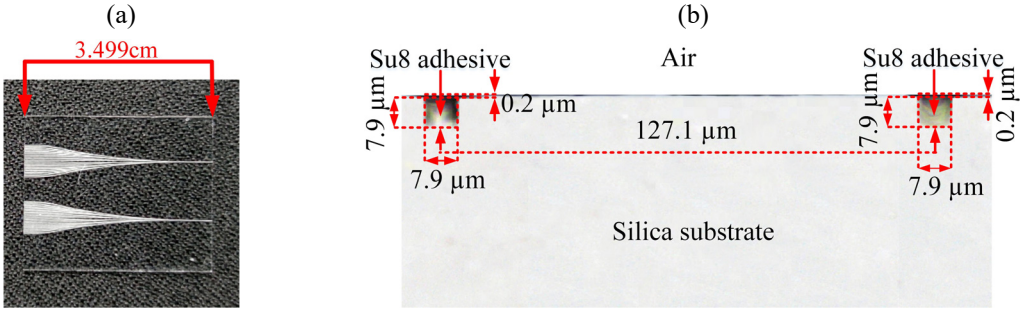

Fig. 13. The 1×32 optical splitter. (a) Top view and details, and (b) cross-sectional view of output ports.

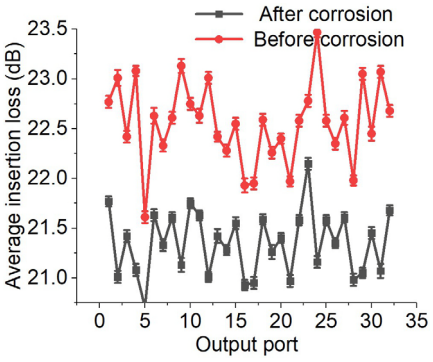

Fig. 14. Average insertion loss of each output port.

1.85 dB in Fig. 14. By comparison, it was easily found that the average insertion loss of each output port was reduced by 1.22 dB, and the uniformity was also reduced by 0.41 dB. Surface roughness was less than or equal to 0.2 μm.

Through above analysis, the optimal ablating parameters were: the laser power 40 mW, translational speed 5 mm/s, center distance *d* between two adjacent ablating lines 0.5 μm. In order to obtain a best groove, a focused beam needed to repeatedly ablate the silica substrate in the same direction. A 5% concentration hydrofluoric acid solution was used to corrode the silica groove for 2 min at 100°C. Surface roughness Ra could be less than 0.2 μm.

5. Conclusions

A composite manufacturing method was used to ablate a silica groove for 1×32 optical splitter. The simulation results shown that average normalized output power of semi -buried Su8 1×32 optical splitter was 18.403 dB and uniformity was 1.265 dB. The testing results shown that the length of 1×32 optical splitter was 3.499 cm, and spacing of output ports was almost 127.1 μm. The average insertion loss of every output ports was 21.34 dB, and uniformity was less than 1.44 dB. Compared with the traditional ablation method, the composite manufacturing method improved the communication performance. This satisfied the requirements of optical interconnection for the EOPCB.

Acknowledgements

This work was supported by Hubei University of Technology Green Industry Technology Leading Project (CPYF2017002); Hubei University of Technology "Advanced Manufacturing Technology and Equipment" Collaborative Innovation Center Open Research Fund (1201501); Hubei University of Technology "Advanced Manufacturing Technology and Equipment" Collaborative Innovation Center Open Research Fund (1201803).

References

[1] ShangGuan L., Zhang D., Zhang T., Cheng R., Wang J., Wang C., Wang F., Ho S.-T., Chen C., Fei T., *Functionalized polymer waveguide optical switching devices integrated with visible optical amplifiers based on an organic gain material*, Dyes and Pigments **176**, 2020: 108210. https://doi.org/10.1016/j.dyepig.2020.108210

[2] Jiang M., Zhang D., Lian T., Wang L., Niu D., Chen C., Li Z., Wang X., *On-chip integrated optical switch based on polymer waveguides*, Optical Materials **97**, 2019: 109386. https://doi.org/10.1016/j.optmat.2019.109386

[3] Giacon V.M., da Silva Padilha G., Bartoli J.R., *Fabrication and characterization of polymeric optical by plasma fluorination process*, Optik **126**(1), 2015: 74-76. https://doi.org/10.1016/j.ijleo.2014.08.152

[4] Nieweglowski K., Lorenz L., Lüngen S., Tiedje T., Wolter K.-J., Bock K., *Optical coupling with flexible polymer waveguides for chip-to-chip interconnects in electronic systems*, Microelectronics Reliability **84**, 2018: 121-126. https://doi.org/10.1016/j.microrel.2018.03.020

[5] De Vittorio M., Todaro M.T., Stomeo T., Cingolani R., Cojoc D., Di Fabrizio E., *Two-dimensional photonic crystal waveguide obtained by e-beam direct writing of SU8-2000 photoresist*, Microelectronic Engineering **73-74**, 2004: 388-391. https://doi.org/10.1016/j.mee.2004.02.075

[6] KO F.-H., CHEN J.-K., CHANG F.-C., *Fabricating and characterizing oblique polymer structures by electron beam writing on resist-coated SiO_2 wafers*, Microelectronic Engineering **83**(4-9), 2006: 1132-1137. https://doi.org/10.1016/j.mee.2006.01.027

[7] KUMAR V.S., TURAGA S.P., TEO E.J., BETTIOL A.A., *Fabrication of optical microresonators using proton beam writing*, Microelectronic Engineering **102**, 2013: 33-35. https://doi.org/10.1016/j.mee.2012.02.017

[8] HUANG L., QIN Y., JIN Y., SHI H., GUO H., XIAO L., JIANG Y., *Spheroidal trap shell beyond diffraction limit induced by nonlinear effects in femtosecond laser trapping*, Nanophotonics **9**(14), 2020: 4315-4325. https://doi.org/10.1515/nanoph-2020-0288

[9] ZHOU K., SHEN F., YIN G., ZHANG L., *Optical fiber micro-devices made with femtosecond laser*, [In] *Advanced Photonics 2016 (IPR, NOMA, Sensors, Networks, SPPCom, SOF)*, OSA Technical Digest (online), Optica Publishing Group, 2016: paper SeW3D.1. https://doi.org/10.1364/SENSORS.2016.SeW3D.1

[10] HEATH D.J., GRANT-JACOB J.A., FEINAEUGLE M., MILLS B., EASON R.W., *Sub-diffraction limit laser ablation via multiple exposures using a digital micromirror device*, Applied Optics **56**(22), 2017: 6398-6404. https://doi.org/10.1364/AO.56.006398

[11] LENG Y., YUN V.E., GOLDHAR J., *UV laser fabrication and modification of fiber Bragg gratings by stitching sub-gratings with in situ fluorescence monitoring*, Applied Optics **56**(24), 2017: 6977-6981. https://doi.org/10.1364/AO.56.006977

[12] MIRZA M.A., STEWART G., *Theory and design of a simple tunable Sagnac loop filter for multiwavelength fiber lasers*, Applied Optics **47**(29), 2008: 5242-5252. https://doi.org/10.1364/AO.47.005242

[13] WANG Y., LI Y., LIAO C., WANG D.N., YANG M., LU P., *High-temperature sensing using miniaturized fiber in-line Mach–Zehnder interferometer*, IEEE Photonics Technology Letters **22**(1), 2009: 39-41. https://doi.org/10.1109/LPT.2009.2035638

[14] DAVIS K.M., MIURA K., SUGIMOTO N., HIRAO K., *Writing waveguides in glass with a femtosecond laser*, Optics Letters **21**(21), 1996: 1729-1731. https://doi.org/10.1364/OL.21.001729

[15] TAO Q., LUO F., YUAN J., SHI L., HU J., DING X., WANG R., CAO L., *Performance analysis of 45° coupled structure of optical waveguide based on electro-optical printed circuit board*, Optik **122**(1), 2011: 76-80. https://doi.org/10.1016/j.ijleo.2010.02.008

[16] TAO Q., LU B., ZHAI Z., CHENG J., LIU D., *Manufacturing a 1 × 16 air-cladding polymeric optical splitter for electro-optical printed circuit boards by femtosecond laser*, Optical Engineering **59**(1), 2020: 017105. https://doi.org/10.1117/1.OE.59.1.017105

[17] MANNION P.T., MAGEE J., COYNE E., O'CONNOR G.M., GLYNN T.J., *The effect of damage accumulation behaviour on ablation thresholds and damage morphology in ultrafast laser micro-machining of common metals in air*, Applied Surface Science **233**(1-4), 2004: 275-287. https://doi.org/10.1016/j.apsusc.2004.03.229

[18] YANG Z., WANG D., YANG D., WANG Y., RONG L., *Optimized design of 1×4 optical splitter based on annealed proton exchanged waveguides in $LiNbO_3$ crystal*, Proceedings of the SPIE, Vol. 9043, International Conference on Optical Instruments and Technology - Optoelectronic Devices and Optical Signal Processing, 2013: 904306. https://doi.org/10.1117/12.2038166

[19] SCHLAAK H.F., BRANDENBURG A., SULZ G., *Integrated optical circuits with curved waveguides*, Proceedings of the SPIE, Vol. 0651, Integrated Optical Circuit Engineering III, 1986: 38-45. https://doi.org/10.1117/12.938127

[20] SUN C., ZHAO J., WANG Z., DU L., HUANG W., *Broadband and high uniformity Y junction optical beam splitter with multimode tapered branch*, Optik **180**, 2019: 866-872. https://doi.org/10.1016/j.ijleo.2018.12.013

[21] SUZUKI K., KONOIKE R., HASEGAWA J., SUDA S., MATSUURA H., IKEDA K., NAMIKI S., KAWASHIMA H., *Low-insertion-loss and power-efficient 32 × 32 silicon photonics switch with extremely high-Δ silica PLC connector*, Journal of Lightwave Technology **37**(1), 2019: 116-122. https://doi.org/10.1109/JLT.2018.2867575

[22] ZAMHARI N., EHSAN A.A., *Large cross-section rib silicon-on-insulator (SOI) S-bend waveguide*, Optik **130**, 2017: 1414-1420. https://doi.org/10.1016/j.ijleo.2016.11.161

[23] BASAK A., DEKA H., MONDAL A., SINGH U.P., *Impact of post-deposition annealing in Cu_2SnS_3 thin film solar cells prepared by doctor blade method*, Vacuum **156**, 2018: 298-301. https://doi.org/10.1016/j.vacuum.2018.07.049

[24] ZHANG H., HEALY N., SHEN L., HUANG C.C., HEWAK D.W., PEACOCK A.C., *Enhanced all-optical modulation in a graphene-coated fibre with low insertion loss*, Scientific Reports **6**, 2016: 23512. https://doi.org/10.1038/srep23512

[25] MOHAMMED P.A., *Integration of self-standing X- and Y- shaped polymer coupler and splitter with single mode optical fibers*, Optical Materials **111**, 2021: 110685. https://doi.org/10.1016/j.optmat.2020.110685

[26] LIN Q., FAN Z.J., WANG W., YAN Z., ZHENG Q., MEI X., *The effect of spot overlap ratio on femtosecond laser planarization processing of SiC ceramics*, Optics and Laser Technology **129**, 2020: 106270. https://doi.org/10.1016/j.optlastec.2020.106270

[27] YANG Y., LOU R., CHEN X., FAN W.-H., BAI J., CAO W., CHENG G., SI J.-H., *Influence of energy fluence and overlapping rate of femtosecond laser on surface roughness of Ti-6Al-4V*, Optical Engineering **58**(10), 2019: 106107. https://doi.org/10.1117/1.OE.58.10.106107

Received April 17, 2022
in revised form July 4, 2022